Islamic Azad University
Mashhad Branch

Taghizadeh-Farahmand and Afsari / Iranian Journal of Earth Sciences 10 (2018) / 11-19

Variation of Lithosphere-Asthenosphere boundary beneath Iran by using S Receiver function

Fataneh Taghizadeh-Farahmand*[1], Narges Afsari[2]

1. Department of Physics, Qom Branch, Islamic Azad University, Qom, Iran
2. Department of Civil engennering, Nowshahr Branch, Islamic Azad University, Nowshahr, Iran

Received 29 April 2016; accepted 20 October 2017

Abstract

The current geological and tectonic setting of Iran is due to the ongoing convergence between the Arabian and Eurasian Plates, which resulted in the formation of the Iranian plateau, mountain building, extensive deformation and seismicity. The Iranian plateau is characterized by various domains including the continental collision and the oceanic plate seduction. Based on S receiver functions are provided a high resolution image of lithosphere beneath Iran. In the present work, we used data from teleseismic events (at epicentral distances between 60°-85° with magnitude over 5.7 (Mb)) recorded from 1995 to 2011 at 53 national permanent short period stations which are located in the different geological zones of Iran. The Sp phase conversion arriving at times ranging between 8.6 and 13.0 s delay time. In order to enhance the conversions and reduce the error of the depth determination, the S receiver functions stacked in bins. Arrival times of Sp phases were converted into depth domain using the IASP91 reference velocity model. A relatively shallow LAB at about 80-90 km depth was observed beneath the whole plateau with some exceptions. A low velocity zone was found at about 100 km beneath the Zagros fold and thrust belt and reaching 130 km beneath the Sanandaj-Sirjan Zone, whereas other tectonic zones are recognized by a thin lithosphere of about 80-90 km. This technique can introduce an error up to 10 km in the LAB depth determination.

Keywords: *Lithosphere-Asthenosphere Boundary, S Receiver Function, Teleseismic Waves, Iran.*

1. Introduction

The Earth's tectonic plates constitute the lithosphere so that no proper understanding of plate tectonics can be achieved without reference to the lithosphere. The lithosphere is generally divided into two different parts. The crust lithosphere includes the upper part of the lithosphere, whereas the mantle lithosphere located in the lower part moves as the high velocity lid on the top of the asthenosphere. Observations of low seismic velocities in the upper mantle are generally associated with the Lithosphere-Asthenosphere Boundary named LAB. This boundary appears as a negative contrast in which the seismic velocities decrease with depth. In contrast to the Moho depth which is usually observed at high resolution by different techniques such as P Receiver Function (PRF) method, the lower boundary of the mantle lithosphere is generally considered not sharp enough to be well observed by seismic body wave observations. The thickness of the lithosphere has been mostly obtained from low resolution surface wave observations. The lithosphere has a global average thickness of 80-100 km, ranging between zero and 200 km beneath mid ocean ridges and stable cratons, respectively. However, the recently developed S Receiver Function (SRF) technique (Li et al. 2004; Kumar et al. 2005) can be optimally used to identify the LAB boundary using higher resolution body waves because this method is free of multiples. This boundary is almost invisible in the PRFs due to the crustal multiples, which arrive at the same time and heavily disturb the time window of the LAB arrival.

Iranian Plateau in Southwest Asia is a mountainous land long looking younger Tertiary fold is formed, and Point of view global tectonics, is part of the Alpine-Himalayan orogenic belt in a compressional area of convergence is two-plate Arabic and Eurasia, making it one of the largest regions of convergent deformation on Earth (Allen et al. 2004). Determining the depth of the crust and upper mantle discontinuities and knowing the details of crust are necessary to understand a more accurate determination of focal depth seismic zone, attenuation relationships, a more realistic model of the Earth's subsurface structure for each region, along with stress and etc. Two basic conditions for the occurrence of earthquakes in such areas are required. First, the presence of brittle materials and second movement that causes an accumulation of stress in the brittle materials. These two factors are lithospheric plates. In order to better understand the evolution of tectonic and geodynamic in each area, investigation of subsurface structure of the earth (crust and upper mantle) is essential.

Despite the numerous studies that have been done on determining the structure of the crust in Iran (Asudeh 1982; Dehghani and Makris 1984; Snyder and Barazangi 1986; Mangino and Priestley 1998; Javan

*Corresponding author.
E-mail address (es): f_farahmand@Qom-iau.ac.ir

Doloei and Roberts 2003; Hatzfeld et al. 2003; Paul et al. 2006; Yamini-Fard et al. 2006; Sodoudi et al. 2009; Radjaeei et al. 2010; Taghizadeh-Farahmand et al. 2010; 2013, 2015; Abbassi et al. 2010; Afsari et al. 2011), there is little information about the structure of lithosphere and there is a few studies on Lithosphere thickness in Iran (Sodoudi et al. 2009; Taghizadeh-Farahmand et al. 2010; Jim'enez-Munt et al. 2012; Priestley et al. 2012; Motavalli-Anbaran et al. 2011; Priestley et al. 2012; Mohammadi, et al. 2013). The recently developed S Receiver Function technique (Farra and Vinnik 2000; Li et al. 2004, Kumar et al. 2005 a, b, 2006, 2007; Sodoudi et al. 2006 a, b,) can be optimally used to identify the lithosphere–asthenosphere boundary (LAB) with higher resolution rather than obtained by body waves.

The main goal of this paper is to derive a high-resolution image of the lithosphere in Iran using S Receiver Functions. According to the location of seismic networks and stations, the study region is divided into seven parts: Alborz (Tehran, Sari and Semnan), Northwest of Zagros (Kermanshah), Central Iran (Yazd and Isfahan), Northwest of Iran (Tabriz), Northeast of Iran (Mashhad and Quchan), Central Zagros (Shiraz) and Eastern of Iran (Birjand). Networks located in any study region are shown in parentheses.

2. Data and Method

The data used for this study were recorded by the Iranian Seismological Center (ISC), which consists of 12 seismic networks with 61 permanent short-period seismic stations (Fig 1). Specifications of the seismic stations are available in the electronic database (http://irsc.ut.ac.ir/istn.php?lang=fa).

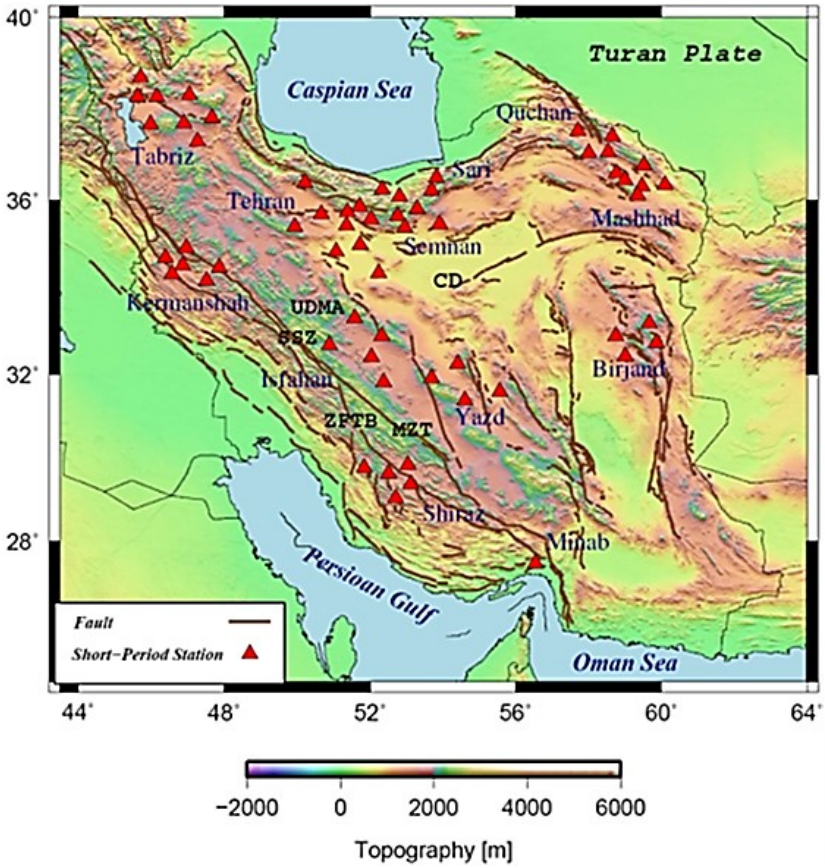

Fig 1. Location map of the seismological stations used in this study with red triangles. Active faults are shown with brown lines (Hessami et al. 2003). Central Domin (CD), Sanandaj-Sirjan Zone (SSZ), Main Zagros Thrust (MZT), Zagros fold and thrust belt (ZFTB), Urumieh–Dokhtar magmatic arc (UDMA).

The short-period networks are operated by the Iranian Seismological Center (ISC). They are equipped with SS-1seismometers with a natural frequency of 1 Hz and sampling rate of 50 samples per second which are made by Nanometrics and connected to the central recording station via a telemetric system. More than 400 teleseismic events (Fig 2) with magnitudes greater than 5.7 (Mb) at epicentral distances between 60˚ and 85˚ have been used for the S Receiver Function analysis. The PRF technique searches the P to S conversions at

seismic discontinuities beneath stations, while SRF analysis looks for the S to P conversions at the seismic discontinuities. A Sp phase is generated when an incoming S phase crosses a velocity discontinuity beneath a seismic station and is converted to the P wave.

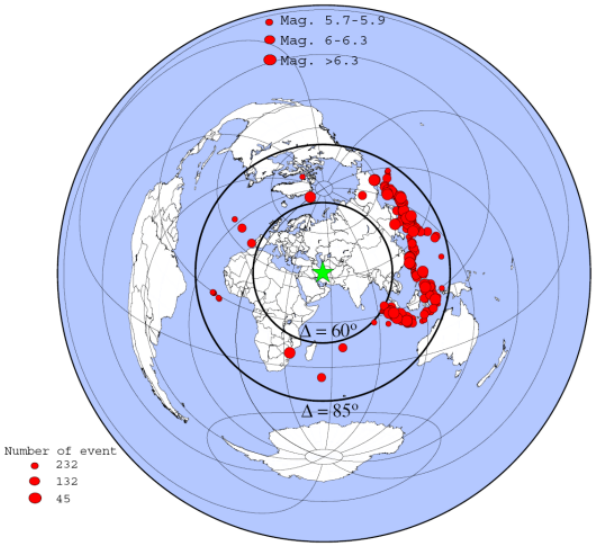

Fig 2. Distribution of teleseismic events (Red solid circles) recorded by the national permanent stations of Iran between 1995 and 2011.The green star represents the approximate position of Iran. The black solid circles mark the 60˚ and 85˚ epicentral distances, respectively.

In a particular station, the converted Sp phase arrives earlier than the direct S phase (e.g. Faber and Müller 1980; Farra and Vinnik 2000; Li et al. 2004; Kumar et al. 2005). Converted Sp phases from shallow discontinuities (like crust-mantle and lithosphere-asthenosphere boundaries) are best observed at epicentral distances between 60-85° (Faber and Müller 1980). S Receiver Functions are primarily much noisier than P Receiver Functions because they arrive after the P wave.

They also have longer periods in comparison with the P Receiver Functions and do not resolve the fine structure within the crust and mantle lithosphere. However, they are precursors to S waves, whereas all the multiple reverberations appear later than S. This advantage having no multiples enables them to separate the primary converted phases from the disturbing multiples, which are not much visible. The boundaries, which are normally covered by multiples arriving at nearly the same time in the P receiver functions, can also be identified in the S Receiver Functions. Calculation of SRFs is similar to that of PRFs and includes restitution, coordinate rotation and deconvolution. For rotation, the angle of incidence is defined by the minimum of energy in the L component at arrival time of the S phase (see also Kumar et al. 2006). Final deconvolving the Q component from the L component results in having the converted S to P phases on the L component. To make the SRF directly comparable with PRF, we reversed the polarity of the S Receiver Function amplitudes as well as the time axis. Prior to summation, moveout correction for a reference slowness of 6.4 s/◦ was essentional.

3. Observation

We selected a time window of 200 s in length (100 s before the S onset) and calculated the S receiver functions (SRF). A low pass filter of 4 s was applied to the data. Only traces with high signal-to-noise ratio (>4) were considered and calculated SRFs for all the stations. As an example, SRFs calculated for two stations (MHI and DMV) are shown in figure 3.

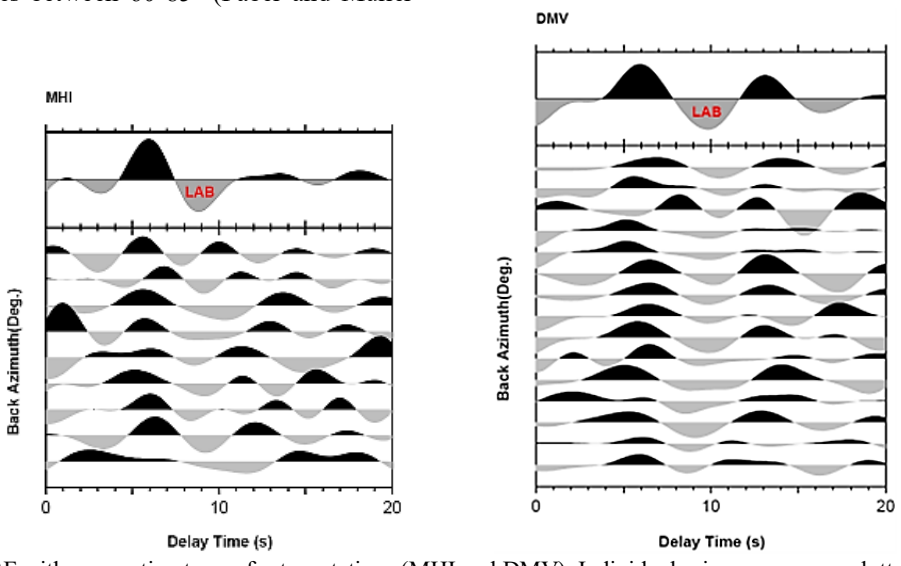

Fig 3. Individual SRF with summation traces for two stations (MHI and DMV). Individual seismograms are plotted equally spaced and sorted by increasing back azimuth. They are filtered with a low pass filter of 4 s. The S onset is fixed at zero time. The clear negative phase at 9-10 s on the summation trace (labeled LAB) is interpreted as the conversion from the LAB.

The S Receiver Functions are sorted by the increasing back azimuth. Negative (positive) amplitudes, plotted in gray (black), indicate a velocity decrease (increase) with depth. Two main phases can be recognized in SRFs; the Moho as a positive peak at 6 s. The S to P conversion from the Moho is well observed at 6 s in good agreement with the PRFs obtained from this station in our previous study (Taghizadeh-Farahmand et al. 2015) and a clear negative peak at times ranging between 9 and 10 s that labeled LAB. This phase may represent the S-to-P conversion at the Lithosphere–Asthenosphere Boundary. The LAB conversion can be isolated in the SRF, since they are free of multiples. Arrival times of LAB phases were converted into depth domain using the IASP91 reference velocity model (Kennett and Engdahl 1991).

4. Discussion

The depth of LAB was investigated by SRF beneath all stations. Figure 4 shows the distribution of the S-to-P piercing points at the depth of 100 (likely to be the approximate thickness of the continental lithosphere).
The S to P conversion points are not located close to the stations. In order to enhance the conversions and reduce the error of the depth determination, the SRFs stacked in bins of 0.1˚ (overlapping factor of 0.05˚) and sorted them by longitude of piercing points the depth of 100 km.

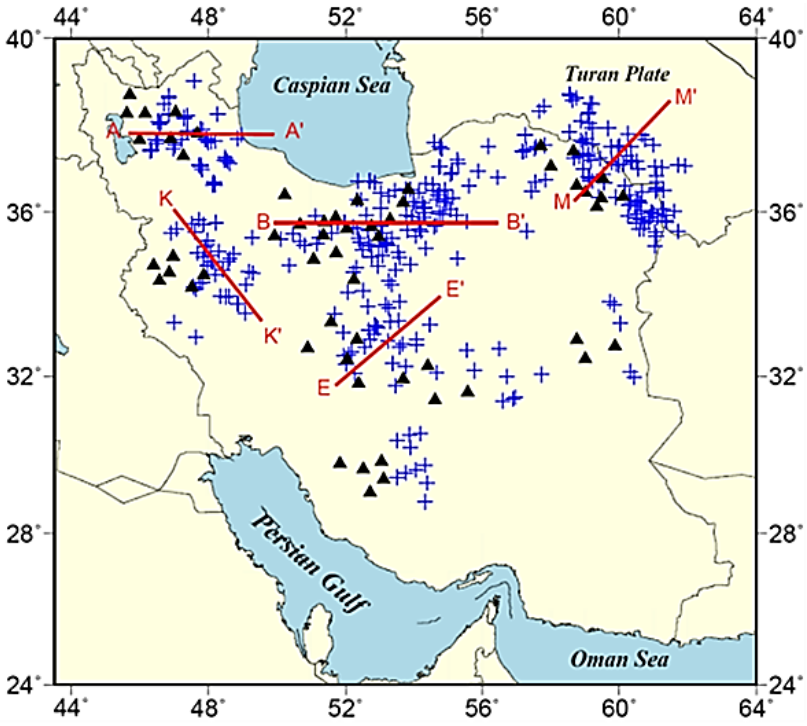

Fig 4. Location of piercing points (blue crosses) of S receiver functions at 100 km depth. Red lines marks the location of the profiles used for Figs. 5 and 6. The seismological stations are shown with black triangles.

Results of stacking for some networks are shown in figure 5a-c. The stacking method gained the S to P conversions by averaging the information of several single SRF within each bin. Negative (positive) amplitudes, plotted in gray (black) indicate a velocity decrease (increase) with depth. In upper panel, two main phases are visible on the summation trace: the first phase which is in blue, at about 6-7 s, is related to the Moho discontinuity. The second phase, which has strong negative amplitude (in red) at ~8.5-9.5 s, may represent the S to P conversion at the Lithosphere–Asthenosphere Boundary (labeled as LAB).

The migrated SRF sections obtained some seismic network (Fig 6a-e) which has enough SRF data. Location of profiles for each network is shown by red line in figure 4. To transform time into the depth, the IASP91 reference model (Kennett and Engdahl 1991) is used. The positive amplitudes of receiver functions are plotted in red, while blue color shows negative amplitudes.
It should be mentioned that the results of each seismic network can't be related to beneath those networks but these results are related to stacking of recorded teleseismic event in each seismic network.

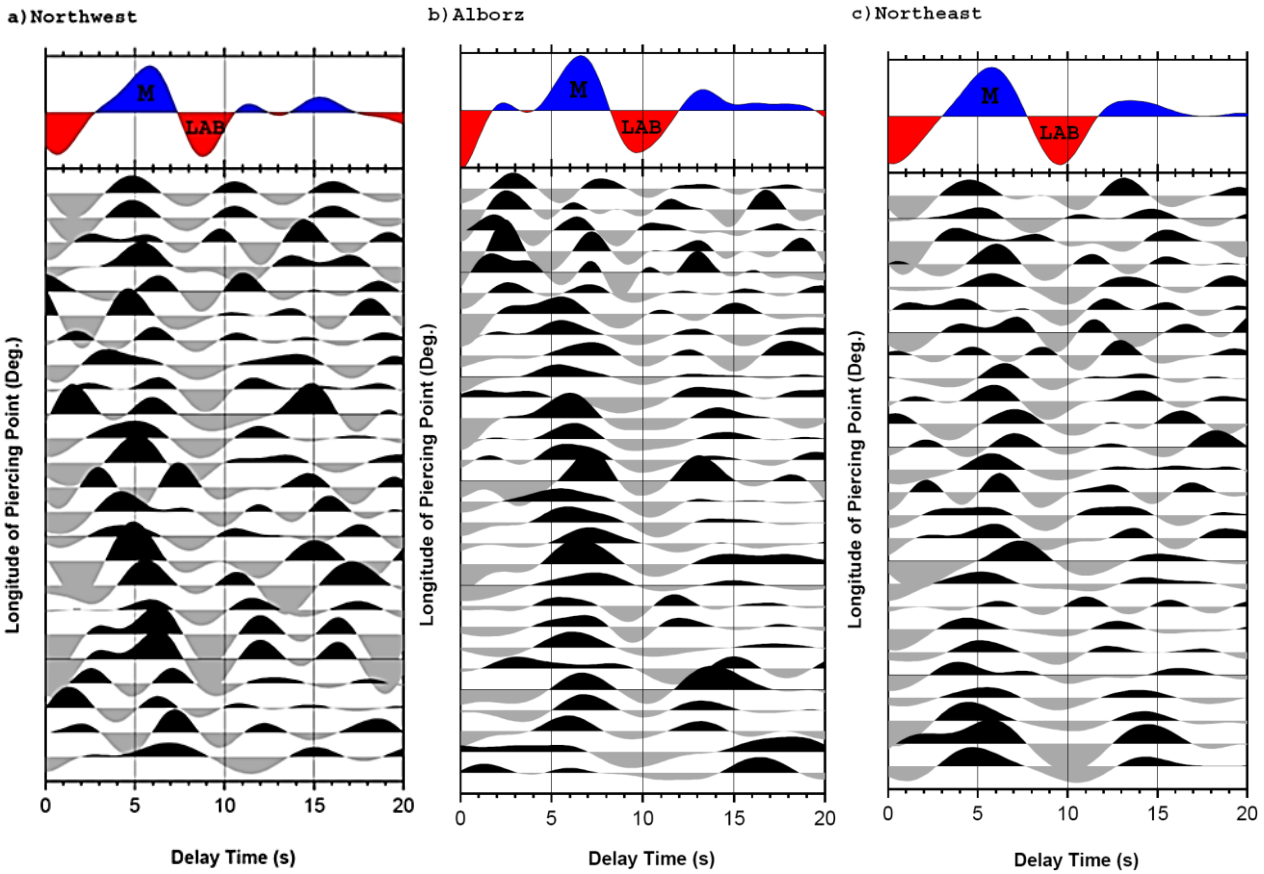

Fig 5. The stacked SRF (in bins of 0.1˚) sorted by longitude of piercing points at 100 km. a) Northwest (Tabriz), b) Alborz (Tehran, Sari and Semnan) and c) Northeast (Mashhad and Quchan). Negative (positive) amplitudes indicate a velocity decrease (increase) with depth and are plotted in gray (black) and white (gray) for the stacked data, respectively. Tow clear Sp conversions are visible in SRF and labeled on the summation trace (Moho and LAB). The strong Sp conversion with the negative amplitude shown in red at ~8.5-9.5 is interpreted as the conversion from the LAB (labeled LAB)).

In SRF, piercing points have lateral offset with station but in PRF the conversion in a cluster and sub-stations are concentrated exactly like (e.g Sodoudi et al. 2009, 2015). Well is seen in Figure 4 that piercing points (blue crosses) are not located beneath the stations and the results calculated (Table 1) as the thickness of the lithosphere or low velocity layer in each region are related to areas in which areas are piercing points. According to Figure 5a for Northwest Iran, arrival time of Sp converted phase of Moho in SRF was about 6 s that is good agreement by our previous study (Taghizadeh-Farahmand et al. 2010, 2015) via P Receiver Function method, as well as the negative phase at the arrival time which was seen about 8.9 seconds (LAB) related to the converted phase Sp of the Lithosphere-Asthenosphere Boundary. In the figure 6a, 2D cross-section of the depth-distance, two discontinuity shows, one (positive polarity) at a depth of 45 to 55 kilometers associated with the Moho and the other (negative polarity) at a depth of about 80 to 100 kilometers of LAB. Tomographic studies (Bayramnejad 2008) estimated a significant LVZ in NW Iran, a depth of about 12 and 15 km for the LVZ beneath the volcanoes, respectively. In this case, a depth of 85 km seems to be very deep for the LVZ and could not be reasonable. Jim´enez-Munt et al. (2012) by residual Bouguer anomalies obtained the average lithospheric thickness beneath NW Iran is 100 to 120 km. Surface waves studies revealed a 100 km deep lithosphere beneath the NW Iran (McKenzie and Priestley 2008, Priestley et al. 2012). By using SRF beneath the eastern Turkey Angus et al. (2006) showed a relatively thin lithosphere beneath this region. According to the error introducing in our S Receiver Function analysis, the LAB depth is in good correlation with those obtained from previous studies.

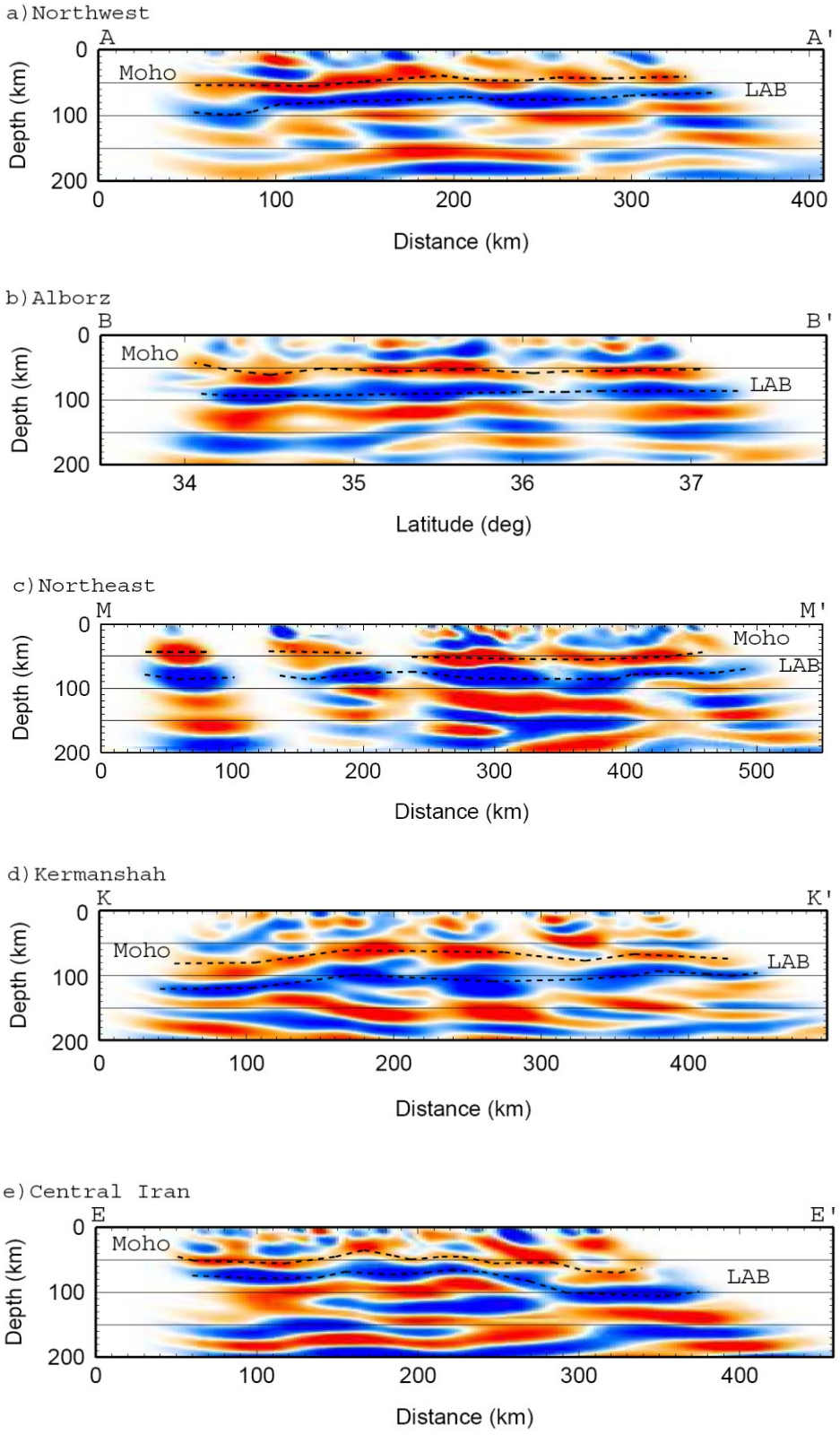

Fig 6. 2D migrated SRFs along profiles AA', BB', MM', KK' and EE' for some seismic networks. a) Northwest (Tabriz), b) Alborz (Tehran, Sari and Semnan), c) Northeast (Mashhad and Quchan), d) Northwest of Zagros (Kermanshah) and e) Central Iran (Yazd and Isfahan). The positive (negative) amplitudes of receiver function are plotted in red (blue). Variation of Moho and LAB thickness are shown by dash line and labeled.

Moho conversion phase by SRF in Alborz region was about 5.6 s which is labeled by M (Fig 5b), the results is in agreement with the arrival time of Ps converted phase in PRFs (6.3 s) (Sodoudi et al. 2009). The result of SRF migrated (Figure 6b) indicates variation of lithospheric thickness between 80-90 km in Alborz region that fits well to the observed stacked data (Fig. 5b). It seems to be relatively thin lithosphere for this high elevated tectonic belt. Sodoudi et al. (2009) suggested this thinning is supported by asthenospheric material. These results are also in good agreement with other geophysical studies beneath the Alborz region (McKenzie and Priestley 2008, Motavalli-Anbaran et al. 2011).

Moho converted phase was seen about 5.8 s in SRF in Northeast Iran (Mashhad and Quchan) (Fig 5c) which is related to 50 to 55 km depth for Moho in 2D cross-section depth and distance (Fig 6c) that is in good agreement with result of modeling via gravity data by Motavalli-Anbaran et al. (2011) (45-48 km) and Jim´enez-Munt et al. (2012) (~50 km). Migrated SRF sections (Fig 6c) significantly map the Moho and the LAB beneath the NE Iran. SRFs stacking clearly map the S-to-P conversions from the LAB at times ranging between 8.5 and 10.5 s (Fig 5c). This arrival times suggest lithospheric thickness of approximately 85–95 km which seems to be relatively thin for NE Iran with relative high topography, which has been undergoing a shortening process in response to the collision of Arabia with Eurasia (e.g., Hollingsworth et al. 2010). It should be noted that the position of the piercing points are far from elevated region and are located in Turan plate. Motaghi et al. (2012) computed the Bouguer anomaly over a profile crossing the Kopeh-Dagh belt. Their modeling showed that the mountain ranges are supported dynamically instead of by the mechanism of isostasy. Previous studies from the phase velocity dispersion of Rayleigh waves by different authors (e.g., McKenzie and Priestley 2008, Priestley et al. 2012), who suggested a thickness of ~100 km for the lithosphere of NE Iran is in good correlation with this study.

Table 1. Strike of Profile or Study Region /Name of network, Arrival time of Sp converted phase (Second), Depth of LAB (Km) and Number of SRF.

Strike of Profile/Study Region	Arrival time of Sp phase (Sec.)	depth of LAB (Km)	Number of SRF
AA'	8.9	80	64
MM'	9.5	85	130
BB'	9.5	85	153
EE'	8.6-11	80-110	60
KK'	10-13	100-130	55
East Iran (Birjand)	9.5	85	15

The migrated SRF sections obtained some seismic network (Fig 6a-e) which has enough SRF data. Location of profiles for each network is shown by red line in figure 4. To transform time into the depth, the IASP91 reference model (Kennett and Engdahl 1991) is used. The positive amplitudes of receiver functions are plotted in red, while blue color shows negative amplitudes.

It should be mentioned that the results of each seismic network can't be related to beneath those networks but these results are related to stacking of recorded teleseismic event in each seismic network. In SRF, piercing points have lateral offset with station but in PRF the conversion in a cluster and sub-stations are concentrated exactly like (e.g. Sodoudi et al. 2009, 2015). Well is seen in Figure 4 that piercing points (blue crosses) are not located beneath the stations and the results calculated (Table 1) as the thickness of the lithosphere or low velocity layer in each region are related to areas in which areas are piercing points.

5. Conclusion

Based on S receiver functions analysis was provided a high resolution image of lithosphere beneath Iran. Data set selected from teleseismic events (Mb>5.7, epicentral distance between 60° and 85°) recorded from 1995 to 2011 at all short period stations of Iranian Seismological Center (ISC). In order to enhance the conversions and reduce the error of the depth determination, the S receiver functions stacked in bins and sorted them by longitude of piercing points. To compare P and S receiver functions, migrated SRF sections obtained along some profiles. Clear image of the LAB has been able to present at depths ranging between 80 km beneath

Central Iran (Yazd) to Maximum 130 km beneath Sanandaj-Sirjan Zone. A relatively thin continental lithosphere of about 80 and 85 km are found beneath the northwest and northeast of Iran, respectively. Furthermore, relatively thick lithosphere of about 130 km is found beneath the SSZ near the Kermanshah region, whereas beneath the Central Zagros (Shiraz) a relatively thin lithosphere was seen. The average thickness of the lithosphere of Alborz is estimated to be 85 km and vary between 90-80 km from west to the east.

Acknowledgements

Authors are grateful to the Iranian Seismological Center (ISC) for providing the teleseismic waveforms. The software packages Seismic Handler (Stammler 1993) used for data processing and GMT (Wessels and Smith 1998) for plotting, respectively. We are thankful of Forough Sodoudi from GFZ Potsdam for her considerable help. This research was supported by the Islamic Azad University, Qom branch.

References

Abbassi A, Nasrabadi A, Tatar M, Yaminifard F, Abbassi M, Hatzfeld D, Priestley K (2010) Crustal velocity structure in the southern edge of the Central Alborz (Iran), *Journal of Geodynamics* 49: 68–78.

Afsari N, Sodoudi F, Taghizadeh-Farahmand F, Ghassemi MR (2011) Crustal structure of Northwest Zagros (Kermanshah) and Central Iran (Yazd and Isfahan) using teleseismic Ps converted phases, *Journal of Seismology* 15: 341–353.

Afsari N, Taghizadeh-Farahmand F, Gheitanchi M R, Solaimani A (2012) Moho depth variations in the Central Zagros (Shiraz region) using Ps converted phases, *Journal of Earth and Space Physics* 38 (3): 1-13.

Allen M, Jackson J, Walker R (2004) Late Cenozoic reorganization of the Arabia-Eurasia collision and comparison of short-term and long-term deformation rates, *Tectonics* 23, TC2008.

Angus DA, Wilson DC, Sandvol E, Ni JF (2006) Lithospheric structure of the Arabian and Eurasian collision zone in eastern Turkey from S-wave receiver functions, *Geophysical Journal International* 166 (3): 1335–1346.

Asudeh I (1982) Seismic structure of Iran from surface and body wave data, *Geophysical Journal International* 71:715-730.

Bayramnejad E (2008) Determination of crustal velocity structure in NW Iran using 3-D inverse modeling of local earthquake data, PhD thesis, Tehran University.

Dehgani GA, Makris J (1984) The Gravity field and crustal structure of Iran, *N. Jb. Geol. Palaeont. Abh*168: 215-229.

Faber S, Müller G (1980) Sp phases from the transition zone between the upper and lower mantle, *Bulletin of the Seismological Society of America* 70: 487-508.

Farra V, Vinnik L (2000) Upper mantle stratification by P and S receiver functions, *Geophysical Journal International* 141: 699-712.

Geissler WH, Sodoudi F, Kind R (2010) Thickness of the central and eastern European lithosphere as seen by S receiver functions, *Geophysical Journal International* 181: 604-634.

Hatzfeld D, MTatar M, Priestley K, Ghafory-Ashtyany M (2003) Seismological constraints on the crustal structure beneath the Zagros mountain belt (Iran), *Geophysical Journal International* 155: 403–410.

Hollingsworth J, Fattahi M, Walker R, Talebian M, Bahroudi A, Bolourchi M J, Jackson J, Copley A (2010) Oroclinal bending, distributed thrust and strike-slip faulting, and the accommodation of Arabia–Eurasia convergence in NE Iran since the Oligocene, *Geophysical Journal International* 181 (3): 1214-1246.

Javan Doloei G, Roberts R (2003) Crust and uppermost mantle structure of Tehran region from analysis of teleseismic P-waveform receiver functions, *Tectonophysics*, 364: 115-133.

Javan Doloei G, Ghafoury Ashtiany M (2004) Crustal structure of Mashhad Area from Time Domain Receiver Functions analysis of teleseismic Earthquake, *Research Bulletin of Seismology and Earthquake Engineering* 27: 30-38.

Jim´enez-Munt I, Fern`andez M, Saura E, Verg´es J, Garcia-Castellanos D (2012) 3-D lithospheric structure and regional/residual Bouguer anomalies in the Arabia–Eurasia collision (Iran), *Geophysical Journal International* 190: 1311–1324.

Kennett BLN, Engdah ER (1991) Travel times for global earthquake location and phase identification, *Geophysical Journal International* 105, 429-465.

Keshvari F, Shomali ZH, Tatar M, Kaviani A (2011) Upper-mantle S-velocity structure across the Zagros collision zone resolved by nonlinear teleseismic tomography, *Journal of Seismology* 15: 329-339.

Kumar P, Kind R, Hanka W, Wylegalla K, Reigber Ch, Yuan X, Wolbern I, Schwintzer P, Fleming K, Dahl-Jensen T, Larsen T B, Schweitzer J, Priestley K, Gudmundsson O, Wolf D (2005a) The lithosphere asthenosphere boundary in the North-West Atlantic region, *Earth and Planetary Science Letters* 236: 249–257.

Kumar P, Kind R, Kosarev G (2005b) The lithosphere-asthenosphere boundary in the Tien Shan-Karakoram region from S receiver functions: evidence for continental subduction, *Geophysical Research Letters* 32 (7): 1-4.

Kumar P, Yuan X, Kind R, Ni J (2006) Imaging the colliding Indian and Asian continental lithospheric plates beneath Tibet, *Journal of Geophysical Research: Solid Earth* 111 (B6): 1-11.

Kumar P, Yuan X, Kumar MR, Kind R, Li X, Chadha R K (2007) The rapid drift of the Indian tectonic plate, *Nature* 449: 894–897.

Laske G (2004) Map of the crustal thickness for Eurasia with 1°×1° resolution, from: http// mahi.uscd.edu/ Gabi/rem.html.

Li X, Kind R, Yuan X, Wolbern I, Hanka W (2004) Rejuvention of the Lithosphere by the Hawaiian plume, *Nature* 427: 827-829.

Mangino S, Priestley K (1998) The crustal structure of the southern Caspian region, *Geophysical Journal International* 133: 630–648.

McKenzie D, Priestley K (2008) The influence of lithospheric thickness variations on continental evolution, *Lithos* 102, 1-11.

Mohammadi N, Sodoudi F, Mohammadi E, Sadidkhouy A (2013) New constraints on lithospheric thickness of the Iranian Plateau using converted waves, *Journal of Seismology* 17 (3): 883-895.

Molinaro M, Zeyen H, Laurencin X (2005) Lithospheric structure beneath the southeastern Zagros Mountains, Iran: recent slab break-off?, *TerraNova* 17: 1-6.

Motaghi, K, Tatar M, Priestley K (2012) Crustal thickness variation across the northeast Iran continental collision zone from teleseismic converted waves. *Journal of seismology* 16: 253–260.

Motavalli-Anbaran SH, Zeyen H, Brunet MF, Ebrahimzadeh Ardestani V (2011) Crustal and lithospheric structure of the Alborz Mountains Iran, and surrounding areas from integrated geophysical modelling, *Tectonic* 30 (5): 1-16.

Nasrabadi A, Tatar M, Kaviani A (2012) Crustal Structure of Iran from Joint Inversion of Receiver Function and Phase Velocity Dispersion of Rayleigh Wave, *Geosciences* 21 (82): 83-94.

Paul A, Hatzfeld D, Kaviani A, Tatar M, Pequegnat C (2010) Seismic imaging of the lithospheric structure of the Zagros mountain belt (Iran), *Geological Society, London, Special Publications* 330: 5-18.

Paul A, Kaviani A, Hatzfeld D, Vegne J, Mokhtari M (2006) Seismological evidence for crustal-scale thrusting in the Zagros mountain belt (Iran), *Geophysical Journal International* 166: 227–237.

Priestley K, McKenzie D, Barron J, Tatar M, Debayle E (2012) The Zagros core: Deformation of the continental lithospheric mantle. *Geochemistry, Geophysics, Geosystems* 13 (11): 1-21.

Radjaee A H, Rham D, Mokhtari M, Tatar M, Priestley K, Hatzfeld D (2010) Variation of Moho depth in the Central part of Alborz Mountains, North of Iran, *Geophysical Journal International* 181: 173–184.

Rajab-biki F, Tagizadeh-Farahmand F, Afsari N, Gheitanchi MR (2011) Variations of the Moho depth and Vp/Vs ratio beneath East Iran (Birjand) using P receiver function method. *Iranian Journal of Geophysics* 5(1): 124-138.

Shad Manaman N, Shomali H (2010) Upper mantle S-velocity structure and Moho depth variations across Zagros belt, Arabian-Eurasian plate boundary, *Physics of the Earth and Planetary Interiors* 180: 92-103.

Shomali Z H, Keshvari F, Hassanzadeh J, Mirzaei N (2011) thospheric structure beneath the Zagros collision zone resolved by non-linear teleseismic tomography, *Geophysical Journal International* 187: 394-406.

Snyder DB, Barazangi M (1986) Deep crustal structure and flexure of the Arabian plate beneath the Zagros collisional mountain belt as inferred from gravity observations, *Tectonics* 5: 361-373.

Sodoudi F, Kind R, Priestly K, Hanka W, Wylegalla K, Stavrakakis G, Vafidis A, Harjes HP, Bohnhoff M (2006a) Lithospheric structure of the Aegean obtained from P and S receiver functions, *Journal of Geophysical Research: Solid Earth* 111 (B12): 12307-12330.

Sodoudi F, Yuan X, Liu Q, Kind R, Chen J (2006b) Lithospheric thickness beneath the Dabie Shan, central eastern China from S receiver functions, *Geophysical Journal International* 166 (3): 1363-1367.

Sodoudi F, Yuan X, Kind R, Heit B, Sadidkhouy A (2009) Evidence for a missing crustal root and a thin lithosphere beneath the Central Alborz by receiver function studies, *Geophysical Journal International* 177(2): 733–742.

Sodoudi F, Yuan X, Asch A, Kind R (2011) High resolution image of the geometry and thickness of the subducting Nazca lithosphere beneath northern Chile, *Journal of Geophysical Research: Solid Earth* 116 (B4): 1-11.

Sodoudi1 F, Brüstle A, Meier T, Kind R, Friederich W, EGELADOS working group (2015) Receiver function images of the Hellenic subduction zone and comparison to microseismicity, *Solid Earth* 6: 135-151.

Taghizadeh-Farahmand F, Sodoudi F, Afsari N, Ghassemi M R (2010) Lithospheric structure of NW Iran from P and S receiver functions, *Journal of Seismology* 14: 823–836.

Taghizadeh-Farahmand F, Sodoudi F, Afsari N, Mohammadi N (2013) A detailed receiver function images of the lithosphere beneath the Kopeh-Dagh (Northeast Iran), *Journal of Seismology* 17(4): 1207-1221.

Taghizadeh-Farahmand F, Afsari N, Sodoudi F (2015) Crustal thickness of Iran inferred from converted waves, *Pure and Applied Geophysics journal* 172(2): 309–331.

Wittlinger G, Farra V, Vergne J (2004) Lithospheric and upper mantle stratification beneath Tibet: New insights from Sp conversions, *Geophysical Research Letters* 31:

Yamini-Fard F, Hatzfeld D, Tatar M, Mokhtari M (2006) Microearthquake seismicity at the intersection between the Kazerun fault and the Main Recent Fault (Zagros, Iran), *Geophysical Journal International* 166 (1): 186-196.